IEEE Access
Multidisciplinary | Rapid Review | Open Access Journal

Received February 25, 2021, accepted March 6, 2021, date of publication March 10, 2021, date of current version March 17, 2021.

Digital Object Identifier 10.1109/ACCESS.2021.3065020

Research on Manipulation Strategy and Flight Test of the Quad Tilt Rotor in Conversion Process

YONGHONG CHEN[1], ZHIGANG WANG[1], ZHICHAO LYU[1], JIANBO LI[2], YONGWEN YANG[1], AND YIBO LI[1]

[1]Yangzhou Academy of Collaboration & Innovation Company Ltd., Yangzhou 225000, China
[2]National Key Laboratory of Rotorcraft Aeromechanics, Nanjing University of Aeronautics and Astronautics, Nanjing 210016, China

Corresponding author: Zhigang Wang (wangzhigang@nuaa.edu.cn)

ABSTRACT The quad tilt rotor (QTR) has the problem of manipulation redundancy due to the helicopter and fixed-wing manipulation mechanisms. Solving the problem of manipulation redundancy and develop an effective manipulation strategy is critical for QTR during conversion flight. A novel manipulation strategy based on states of QTR is proposed in this paper to solve the problem of manipulation redundancy in conversion mode. The longitude is controlled by the tilt angle of nacelle in helicopter mode and the course is controlled by the speed error of propellers in fixed-wing mode. The Active Disturbance Rejection Control (ADRC) is adopt into the flight control law, which can observe and compensate for internal and external disturbance. The simulation and flight test are carried out to verify the proposed manipulation strategy and the results show that the proposed manipulation strategy is effective and reasonable.

INDEX TERMS Quad tilt rotor, manipulation redundancy, manipulation strategy, conversion corridor, flight test.

I. INTRODUCTION

The Quad Tilt Rotor (QTR) [1]–[3] Unmanned Aerial Vehicle (UAV) is a novel vehicle which has the advantages of both fixed-wing and helicopter. It has the Vertical Take Off and Landing (VTOL) performance of a helicopter. At the same time, it has the characteristics of high cruising velocity of a fixed-wing. The QTR has three flight modes [4]: helicopter mode, fixed-wing mode and conversion mode. Its outstanding feature is that there is a tiltable nacelle at each end of the wing. When flying in helicopter mode, the nacelle is perpendicular to the fuselage at an angle of 90°. The propellers provide lift and attitude control torque for the aircraft . When flying in conversion mode, the nacelle gradually tilts forward, and the tilt angle changes from 90° to 0°. The velocity of QTR gradually increases, and the lift of QTR is gradually provided by wings. In conversion mode, the attitude of QTR is controlled by the propellers and the aircraft rudder surface. When the nacelle tilts to horizontal position, the aircraft turns to fixed-wing mode. The propellers only provide the forward pulling force of the aircraft, the lift provided by the wings counteracts the gravity of the aircraft, and the attitude of the aircraft is controlled by the rudder surface. The flight control system of the QTR UAV is very complicated, especially the design of the manipulation strategy in the conversion mode is an important research topic [5]–[8].

QTR UAV has both helicopter and fixed-wing manipulation surfaces, and gradually transforms with the change of nacelle tilt angle. The QTR can be controlled in the same state by helicopter or fixed wing control mechanism and the nacelle. Therefore, the manipulation redundancy of QTR will appear so it has the problem of manipulation redundancy. In view of the multi-flight mode control and distribution of Tilt Rotor (TR) UAVs, the main method currently used is that the lift is provided by the rotor in the helicopter mode, and the lift is mainly provided by the wing in the fixed-wing mode. In the conversion mode, the lift is transitioned from the rotor to the wing by reasonably assigning the control authority. The minimum forward flight speed of the TR UAV and the power provided by the rotor determine the tilt conversion corridor of the TR UAV. In the tilt conversion corridor, choosing an

The associate editor coordinating the review of this manuscript and approving it for publication was Ton Duc Do.

optimal tilt path is essential for the TR UAV to complete a safe and stable conversion flight [9]–[14].

To achieve the mode conversion of a dual tilt rotor unmanned aerial vehicle (dual-TRUAV) from helicopter mode to fixed-wing mode, Zheng [15] *et al.* focused on its conversion control method based on necessary dynamic analysis. With the influence of the tilt angle on dual-TRUAV dynamics analysis, the conversion control strategy based on the tilt angle was established. Sakai and Abiko [16] developed a seamless attitude conversion control method and verified with numerical simulation. Aiming at the problem of manipulation redundancy , Wang *et al.* [17] studied the rudder surface allocation strategy and control channel switching strategy of the aircraft in conversion mode, and developed an attitude controller which designed based on active disturbance rejection control (ADRC) [18]–[21]. They assign the control authority of the rudder surface and the rotor according to the trigonometric function. According to the forward speed and vertical speed, a control channel switching strategy related to the tilt angle is designed. Before starting the conversion mode, the forward speed must be accelerated to 15m/s. However, there is no discussion of conversion directly from hover. Zhang and Lu [22], Zhang *et al.* [23] analyzed the manipulation strategy based on fuzzy control for the manipulation redundancy of the TR. They divided the tilting phase into two stages. When the tilting angle is less than 45°, it is defined as the low-speed phase, and when the tilting angle is greater than 45°, it is defined as the high-speed phase. The helicopter control mode is adopted in the low-speed stage, and the fixed-wing control mode is adopted in the high-speed stage. After adopting fuzzy control to control the nacelle's tilting speed, the height change is reduced from the original 30m to 10m, but the height change is still large for small TRs. Xia *et al.* [24] and others established nonlinear aerodynamic models and flight dynamics models for TR UAVs, and analyzed the full-mode control characteristics, and obtained the control efficiency according to the trim analysis and linearization processing. A set of maneuvering strategies suitable for all modes is proposed. Based on the results obtained from the manipulation efficiency analysis, they assigned a linear control authority to a single channel based on the forward flight speed, and used Proportion Integral Differential (PID) control methods to simulate and verify the four channels. Their research results show that the problem of control redundancy can be effectively solved through linear control authority assignment related to forward flight speed. The above documents basically rely on experience to solve the problem of control redundancy, Yan and Chen [25] introduced the hybrid control equation into the longitudinal flight dynamics model to avoid the jump and discontinuity in the optimization process for the XV-15 TR aircraft. The conversion process is transformed into a nonlinear dynamic optimal control problem, and the direct conversion method and sequential quadratic programming algorithm are used to solve the optimal control problem. During the optimization process, they used altitude, pitch angle, and angular velocity as constraints, and simulated the conversion process of XV-15 from forward and reverse tilt. The results show that the optimized control strategy can make the pitch angle change more smoothly during the conversion process.

It can be seen from the summary analysis of the above-mentioned documents that the current solution to the control redundancy and control strategy of the TR mainly relies on experience to assign a predetermined control factor. Decoupling control of the control surface is realized by assigning authority for control in different flight states. Regarding the tilting path, it is basically to ensure that the tilting angular speed of the TR is within the conversion corridor when the TR in conversion flight mode. The optimal tilting path is not selected based on the control strategy. Therefore, it is necessary to propose a tilt path optimization strategy that comprehensively considers the control strategy to realize the stable and rapid state transition of the TR UAV during the conversion flight.

All of the researches are focus on the general tilt rotor [26], [27]. The tilt rotor aircraft has the problem of rotor and wing aerodynamic interference. In the hovering state, the downwash of the rotor hits the wing directly, which will lead to excessive power consumption in the hovering stage. The hovering stage is one of the main working state of the tilt rotor aircraft. The flight time of the tilt rotor without the tilt wing is greatly shortened. In order to solve the problem above, we design a tilt rotor with partial tilt wing. The design of tilt wing is beneficial to reduce the downwash of the rotor to the wing in hovering mode.

In this paper, the dynamic model of quad tilt rotor with partial tilt wing was established based on Goldstein vortex theory to obtain the conversion corridor. Then, a novel manipulation strategy was proposed to keep the altitude with shortest tilting time in conversion process. Another three manipulation strategy were developed and ADRC algorithm was used to compare with the proposed manipulation strategy. Finally, the simulation and flight test were carried out to verify the proposed manipulation strategy.

The main contributions in this manuscript are list below:

1) To avoid the ''fountain effect'' [28]in helicopter mode, the partial tilt wing is designed for the novel quad tilt rotor.
2) Based on the conversion corridor, a novel manipulation strategy is proposed. The altitude, forward velocity and tilt angle are introduced into the manipulation strategy to ensure the stability of the altitude and attitude in conversion process.
3) In helicopter mode, the QTR is moved horizontally by the nacelle tilting, which ensures that the fuselage is always at a positive angle of attack and the wings always provide effective lift. In the fixed-wing mode, the course control is realized by the difference of propeller pull on both sides of the fuselage, which can increase the efficiency of course control and reduce the rudder, making the structure simpler.

(a) helicopter mode (b) fixed-wing mode

FIGURE 1. 3D model of quad tilt rotor with partial tilt wing.

TABLE 1. Parameters of the quad tilt rotor with partial tilt wing.

category	item	value	
propeller parameter	radius(inch)	20	
	Blade number	2	
	Thread pitch(inch)	12	
Wing parameter		front	rear
	Wing area(m^2)	0.28	0.475
	Tilt wing area(m^2)	0.0425(one side)	
	wingspan(m)	1.3	1.8
	Taper ratio	1.2	1.5
	Mean-chord(m)	0.265	0.3
	Aspect ratio	4.9	6
	Airfoil profile	Eppler1200	
Fuselage parameter	length(m)	1.8	
	Maximum cross-sectional area (m^2)	0.06	
Relative position parameter	Vertical distance of front and rear wings (m)	0.08	
	Vertical distance of the two propellers on the same side(m)	0.08	
	Horizontal distance of the two propellers on the same side(m)	0.26	

4) In order to effectively verify the manipulation strategy proposed in this paper, a prototype aircraft are designed. Both the simulation and flight test results show that the manipulation strategy proposed in this paper can solve the manipulation redundancy in conversion mode very well, and the proposed tilting path can ensure the stability of the altitude and attitude in conversion corridor.

Section II shows the dynamic model of quad tilt rotor. Section III describes the conversion corridor. Section IV shows the manipulation strategy. Section V describes the flight control law. Section VI shows the results and discussions of simulation and flight test. Finally, section VIII draws some conclusions for this paper.

II. DYNAMIC MODEL OF QUAD TILT ROTOR

The quad tilt rotor with partial tilt wing in this paper is shown in Figure 1. The parameters of the quad tilt rotor with partial tilt wing is shown in Table 1. The complexity of the mathematical model is related to the purpose, precision and application of the model. The more detailed the description model is, the more complex the model will be, and the difficulty of solving the model and the application cost of the model will increase accordingly. Therefore, it is necessary to compromise the precision and applicability of the model when establishing the mathematical model. Therefore, before establishing the QTR flight dynamics model, the following assumptions were made:

1) The ground is assumed to be inertial reference system, that is, the ground coordinates are assumed to be inertial coordinates.
2) Think of the earth as flat regardless of the curvature of the earth.
3) The acceleration of gravity and the density of air do not change with altitude.
4) QTR is a rigid body and the mass of the QTR is constant.
5) The blade is rigid, with linear torsion.
6) Compressibility and airflow separation are not considered, and the reflux region is ignored.
7) Aerodynamic interference between the QTR left and right rotors is not considered.
8) QTR has a longitudinal symmetric plane, the $O_bX_bZ_b$ plane of the body coordinate system is a QTR symmetric plane, and the product of inertia $I_{xy} = I_{yz} = 0$.
9) QTR is off the ground.

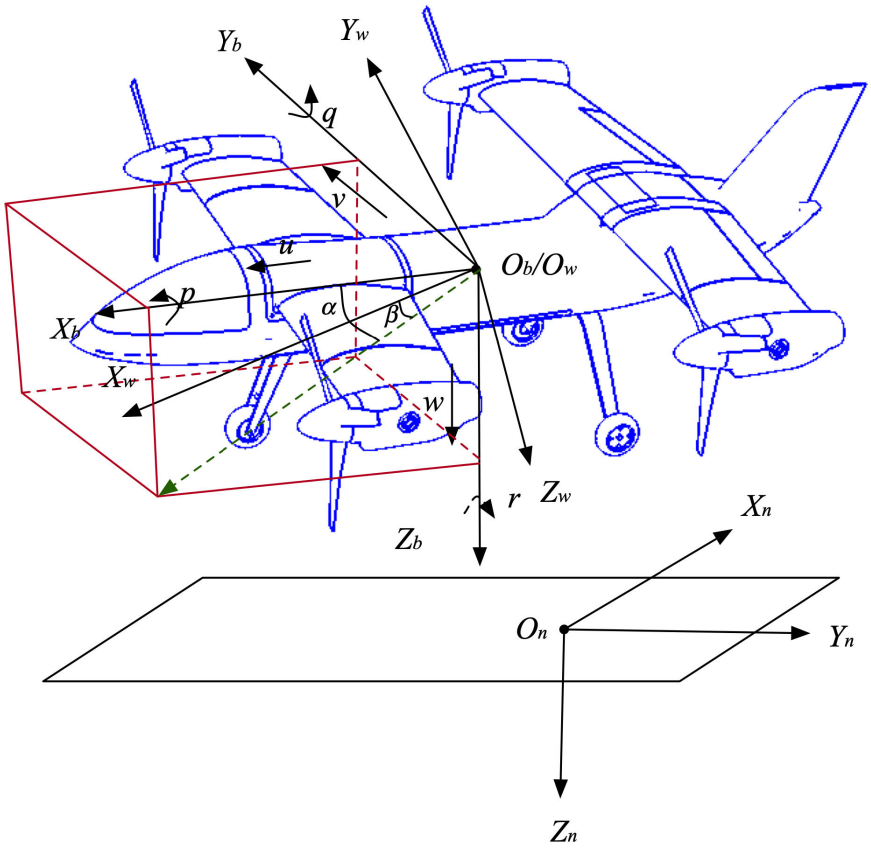

FIGURE 2. Earth/Body/Wind coordinate system.

A. COORDINATE AXIS

The equations of motion for any system are established for a particular reference coordinate. In this paper, the earth coordinate system, body coordinate system, wind coordinate system, nacelle coordinate system, propeller coordinate system and hub-wind coordinate system will be used in the establishment of QTR flight dynamics mathematical model as shown in Figure 2 and Figure 3.

1) EARTH COORDINATE AXIS

The earth coordinate system, also known as the navigation coordinate system or the ground coordinate system, is fixed on the ground of the coordinate system, its origin and axes are defined as follows: The origin (denoted as O_n) is fixed to any point on the ground; The X axis (denoted as X_n) points to the geographic North Pole; The Y axis (denoted as Y_n) points to the east; The Z axis (denoted as Z_n) points downwards along the ellipsoid normal.

Position coordinate vector $\boldsymbol{P_n}$, velocity coordinate vector $\boldsymbol{V_n}$, and acceleration coordinate vector $\boldsymbol{a_n}$ are respectively defined as:

$$\boldsymbol{P_n} = \begin{pmatrix} x_n \\ y_n \\ z_n \end{pmatrix}, \boldsymbol{V_n} = \begin{pmatrix} u_n \\ v_n \\ w_n \end{pmatrix}, \boldsymbol{a_n} = \begin{pmatrix} a_{x,n} \\ a_{y,n} \\ a_{z,n} \end{pmatrix} \tag{1}$$

For simplicity, the following position vector symbols of the earth coordinate system are used throughout this article:

$$\boldsymbol{P_n} = \begin{pmatrix} x \\ y \\ z \end{pmatrix} \tag{2}$$

In addition, $h = -z$ is used to represent the actual flight altitude of the UAV system.

2) BODY COORDINATE AXIS

The body axis coordinate system is fixed to the aircraft and directly defined on the airframe. The origin and each coordinate axis are defined as follows: The origin (denoted as O_b) is the center of gravity(CG) of the aircraft; X axis (denoted as X_b) is located in the longitudinal symmetry plane of the aircraft and points to the nose of the aircraft; Z axis (denoted as Z_b) is located in the longitudinal symmetry plane of the aircraft and points to the abdomen of the aircraft; Y axis (denoted as Y_b) points to the right side of the fuselage and forms the right hand rule with X axis and Z axis.

The velocity coordinate vector $\boldsymbol{V_b}$ and the acceleration coordinate vector $\boldsymbol{a_b}$ are defined as follows:

$$\boldsymbol{V_b} = \begin{pmatrix} u \\ v \\ w \end{pmatrix}, \boldsymbol{a_b} = \begin{pmatrix} a_x \\ a_y \\ a_z \end{pmatrix} \tag{3}$$

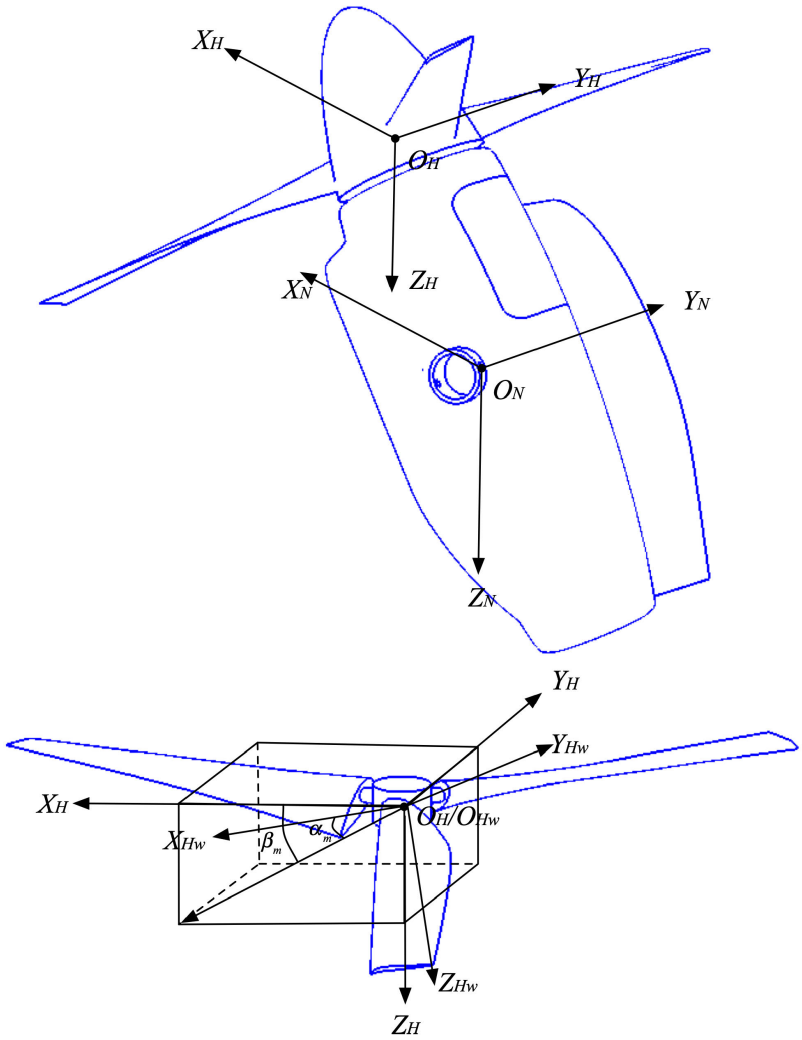

FIGURE 3. Nacelle/Propeller/Hub-wind coordinate system.

3) WIND COORDINATE AXIS

The wind axis coordinate system is fixed on the aircraft, and its origin and coordinate axes are defined as follows: The origin (denoted as O_w) is at the aerodynamic center of all parts of the aircraft; The axis of X (denoted as X_w) is the direction of air flow; Z axis (denoted as Z_w) is perpendicular to the incoming flow direction and points below the fuselage in the longitudinal symmetric plane; The Y axis (denoted as Y_w) points to the right and forms the right hand rule with the X axis and the Z axis.

The lateral slip Angle β is the Angle between the axis of O_wX_w and the plane of $X_bO_bZ_b$, which is positive to the right; the aerodynamic Angle of attack α is the Angle between the velocity vector in the plane of $X_bO_bZ_b$ and the plane of $X_bO_bY_b$, which is positive downward.

4) NACELLE COORDINATE AXIS

The nacelle coordinate system is attached to the nacelles at each end of the wing, with the origin and axes defined as follows: The origin (denoted as O_N) is fixed at the fulcrum of the nacelles at each end of the wing; The X axis (denoted as X_N) points to the front in the longitudinal plane of the entire nacelles; Y axis (denoted as Y_N) is perpendicular to the nacelles longitudinal plane, pointing to the right; The Z axis (denoted as Z_N) forms the right hand rule with the X axis and the Y axis.

The start of the nacelle axis coordinate system is defined at $\beta_m = 90°$, where β_m is the nacelle tilt angle. The nacelle coordinate system moves with the nacelles.

5) PROPELLER COORDINATE AXIS

The coordinate system of the propeller is firmly connected with the hub of the aircraft propeller. The origin and each coordinate axis are defined as follows: The origin (denoted as O_H) is fixed at the hub center at both ends of the wing; X axis (denoted as X_H) points to the front end in the longitudinal plane of the entire paddle disk; Yaxis (denoted as Y_H) is perpendicular to the longitudinal plane of the paddle disk, pointing to the right; The Z axis (denoted as Z_H) forms the right hand rule with the X axis and the Y axis.

The start of the propeller axis coordinate system is defined at $\beta_m = 90°$, where β_m is the nacelle tilt angle. The nacelle coordinate system moves with the nacelles.

6) HUB-WIND COORDINATE AXIS

The hub-wind axis coordinate system is fixed on the hub, and its origin and each coordinate axis are defined as follows: The origin (denoted as O_{Hw}) is in the center of the aircraft hub; The axis of X (denoted as X_{Hw}) is the direction of air flow; Z axis (denoted as Z_{Hw}) is perpendicular to the incoming flow direction and points below the fuselage in the longitudinal symmetric plane; The Y axis (denoted as Y_{Hw}) points to the right and forms the right hand rule with the X axis and the Z axis.

B. FLIGHT DYNAMICS MODEL OF QUAD TILT ROTOR

The dynamic and kinematics equation [29] are shown in equation (4) and equation (5), as shown at the bottom of the next page. Where, m is the weight of aircraft, I is the inertia matrix, u, v, w is the velocity, ϕ, θ, ψ is the euler Angle, p, q, r is the angular velocity.

III. CONVERSION CORRIDOR

The QTR is similar to a quad rotor in helicopter mode. The propeller is the main lift surface. In the fixed-wing mode, the wing is the lifting surface. During the tilt transition flight, the propeller tilts with the nacelle. At this time, the propeller and the wing share the weight of the aircraft, and the pulling force is provided by the forward component of the tilt of the propeller. When tilting with low forward speed, the wing may stall. When tilting with high forward speed, it is limited by factors such as the available power of the propeller and the dynamic stability.

A. NACELLE TILT ANGLE-SPEED ENVELOPE WITH LOW FORWARD SPEED

Nacelle tilt angle-speed envelope with low forward speed is the minimum stall speed of the wing when nacelle starts from hovering in helicopter mode until the fixed-wing mode. Figure 4 shows the force acting on the mass center of the QTR when the nacelle is tilted. In the figure, the $s - s$ plane is the plane of the propeller hub, V is the forward flight speed, α_f is the airframe angle of attack, T is the propeller pull, G is the weight of the aircraft, L and D are respectively body lift and drag.

According to Figure 4, the following force balance relationship can be obtained:

$$T\sin(i_n + \alpha_f) + L = G \tag{6}$$

$$T\cos(i_n + \alpha_f) = D \tag{7}$$

The lift L and drag D in the above two equations can be expressed as:

$$L = L_w = \frac{1}{2}\rho V^2 C_{lw} S_w \tag{8}$$

$$D = D_w + D_f = \frac{1}{2}\rho V^2 C_{dw} S_w + \frac{1}{2}\rho V^2 C_{df} S_f \tag{9}$$

where, L_w and D_w is the lift and drag of wing, D_f is the drag of fuselage, ρ is the density of air, S_w and S_f are the area of wing and fuselage, C_{df} is the drag coefficient of fuselage, C_{lw} and C_{dw} are the lift and drag coefficient of wing. Both of C_{df} and C_{dw} are the function of tilt angle i_n, attack angle of wing α_w, wing flap / aileron status F_x and flying Mach Ma, ie:

$$C_{lw} = f(i_n, \alpha_w, F_x, Ma) \tag{10}$$

$$C_{dw} = f(i_n, \alpha_w, F_x, Ma) \tag{11}$$

During the conversion flight of a TR aircraft, the gravity of the aircraft transitions from the rotor to the wing. When tilting at low speed, the lift provided by the wing is limited by the critical stall attack angle of the wing. Therefore, when calculating the low-speed section tilt envelope, the wing's attack angle is taken as the wing critical angle attack. The wing attack angle and the fuselage attack angle satisfy the following relationship:

$$\alpha_w = \alpha_{lj} = i_w + \alpha_f \tag{12}$$

where, α_{lj} is the wing critical angle attack, i_w is the wing installation angle.

B. NACELLE TILT ANGLE-SPEED ENVELOPE WITH HIGH FORWARD SPEED

When the nacelle of a TR aircraft tilts at high speed, it must not only satisfy the balance of lift and the gravity, but also the horizontal pull component caused by the tilting of the rotor and the drag. At the same time, it must make sure that the rotor has enough available power during the tilting process.

The rotor required power P_r is composed of four parts: induced power P_i, type resistance power P_{pr}, waste resistance power P_p and climb power P_c, namely:

$$P_r = \frac{2}{\eta_p}(P_i + P_{pr} + P_p + P_c) \tag{13}$$

where, η_p is the transmission loss coefficient from the engine to the rotor.

According to the momentum theorem [30] and the principle of conservation of energy, the analytical formulae of induced power P_i, waste resistance power P_p and climb power P_c can be expressed as:

$$P_{ipc} = T(U_c + v_i) \tag{14}$$

where, U_c is the speed perpendicular to the plane of the rotor, and v_i is the induced speed of the rotor.

In order to consider the non-uniformity of rotor induced speed, this paper uses the coefficient K_{ind} to modify it, and its value is 1.15 [31]. Then the equation (14) becomes:

$$P_{ipc} = T(U_c + K_{ind} v_i) \tag{15}$$

According to blade theory [30], the type resistance power of the rotor is:

$$P_{pr} = P_{pr0}(1 + 4.7\mu^2) \tag{16}$$

where, $P_{pr0} = \sigma\pi R^2 \rho V_t^3 c_d/8$, σ is the rotor solidity, c_d is the drag coefficient of blade, V_t is the rotor tip speed, Ω is the

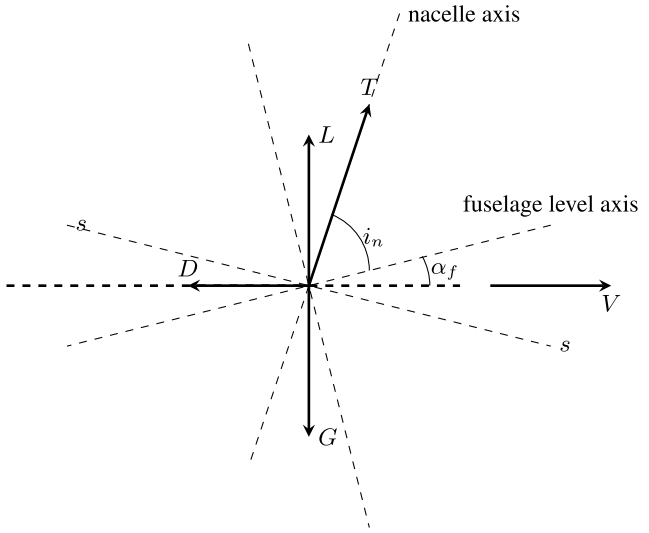

FIGURE 4. The force acting on the mass center of the QTR.

rotor spinning speed, rotor forward ratio is $\mu = U_t/(\Omega R)$, U_t is the speed parallel to the rotor plane.

Define the rotor lift coefficient C_T and power coefficient C_P as:

$$C_T = \frac{T}{\frac{1}{2}\rho\pi R^2 V_t^2} \tag{17}$$

$$C_P = \frac{P}{\frac{1}{2}\rho\pi R^2 V_t^3} \tag{18}$$

Then the rotor power coefficient can be further expressed as:

$$C_T = \frac{1}{2}C_T^{3/2}(\bar{U}_c + K_{ind}\bar{v}_i) + \frac{1}{4}\sigma c_d(1 + 4.7\mu^2) \tag{19}$$

where, $\bar{U}_c = U_c/v_h$, $\bar{v}_i = v_i/v_h$ and $v_h = \sqrt{T/(2\rho\pi R^2)}$ is the rotor characteristic induced speed.

Define $\bar{U}_t = U_t/v_h$, according to the momentum theory, the rotor induced speed satisfies the following formula:

$$\bar{v}_i^4 + 2\bar{U}_c\bar{v}_i^3 + (\bar{U}_c^2 + \bar{U}_t^2)\bar{v}_i^2 = 1 \tag{20}$$

From equation (13) and equation (18), the total required power of the rotor is:

$$P_r = \frac{1}{\eta_p}\rho\pi R^2(\Omega R)^3 C_P \tag{21}$$

In this way, the nacelle tilting angle-speed envelope boundary of the high-speed section of the TR aircraft satisfies the force balance relationship while the total required power of the rotor cannot exceed the rated power P_n of the engine output, namely

$$P_r \le P_n \tag{22}$$

C. CALCULATION PROCESS

Equations (6) and (7) are the balance equations for calculating the conversion corridor of the TR aircraft. The two equations can solve the two unknowns.

When calculating the low-speed nacelle tilt angle-speed envelope, the rotor lift and nacelle angle are the unknown quantities, and when calculating the high-speed nacelle tilt angle-speed envelope, the rotor lift coefficient and the fuselage attitude angle are used as the solution. The specific calculation process is shown in Figure 5. First, obtain the starting point of the low-speed section tilt angle-speed envelope. According to the wing non-stall condition equation (12), at different flight speeds, calculate the wing and fuselage aerodynamic forces of equation (8) and (9) and substitute them into the balance equations (6) and (7). Taking the rotor lift and nacelle angle as unknown quantities, using Newton's method for trim calculation, obtain the low-speed tilt angle-speed envelope of the TR aircraft. When calculating the tilt angle-speed envelope of the high-speed section, set the nacelle angle of TR, use Newton's method to calculate the balance equations (6) and (7). According to equation (21), obtain the value of the rotor required power changed with the forward flight speed, and then according to the engine output power limit condition formula (22), obtain the tilt angle-speed envelope of the TR aircraft at high speed.

Figure 6 shows the calculated tilt conversion corridor of the QTR with partial tilt wing. Where, the black line is the tilt angle-speed envelope at high speed and the red line is the tilt angle-speed envelope at low speed. It can be seen

$$\begin{cases} F_x = m(\dot{u} + qw - rv) + mg\sin\theta \\ F_y = m(\dot{v} + ru - pw) - mg\cos\theta\sin\phi \\ F_z = m(\dot{w} + pv - qu) - mg\cos\theta\cos\phi \\ M_x = I_{xx}\dot{p} - (I_{yy} - I_{zz})qr + I_{yz}(r^2 - q^2) - I_{xz}(pq + \dot{r}) + I_{xy}(pr - \dot{q}) \\ M_y = I_{yy}\dot{q} - (I_{zz} - I_{xx})pr + I_{xz}(p^2 - r^2) - I_{xy}(qr - \dot{p}) + I_{yz}(pq - \dot{r}) \\ M_z = I_{zz}\dot{r} - (I_{xx} - I_{yy})pq + I_{xy}(q^2 - p^2) - I_{yz}(pr - \dot{q}) + I_{xz}(qr - \dot{p}) \end{cases} \tag{4}$$

$$\begin{cases} p = \dot{\phi} - \dot{\psi}\sin\theta \\ q = \dot{\theta}\cos\phi + \dot{\psi}\sin\phi\cos\theta \\ r = -\dot{\theta}\sin\phi + \dot{\psi}\cos\phi\cos\theta \end{cases} \tag{5}$$

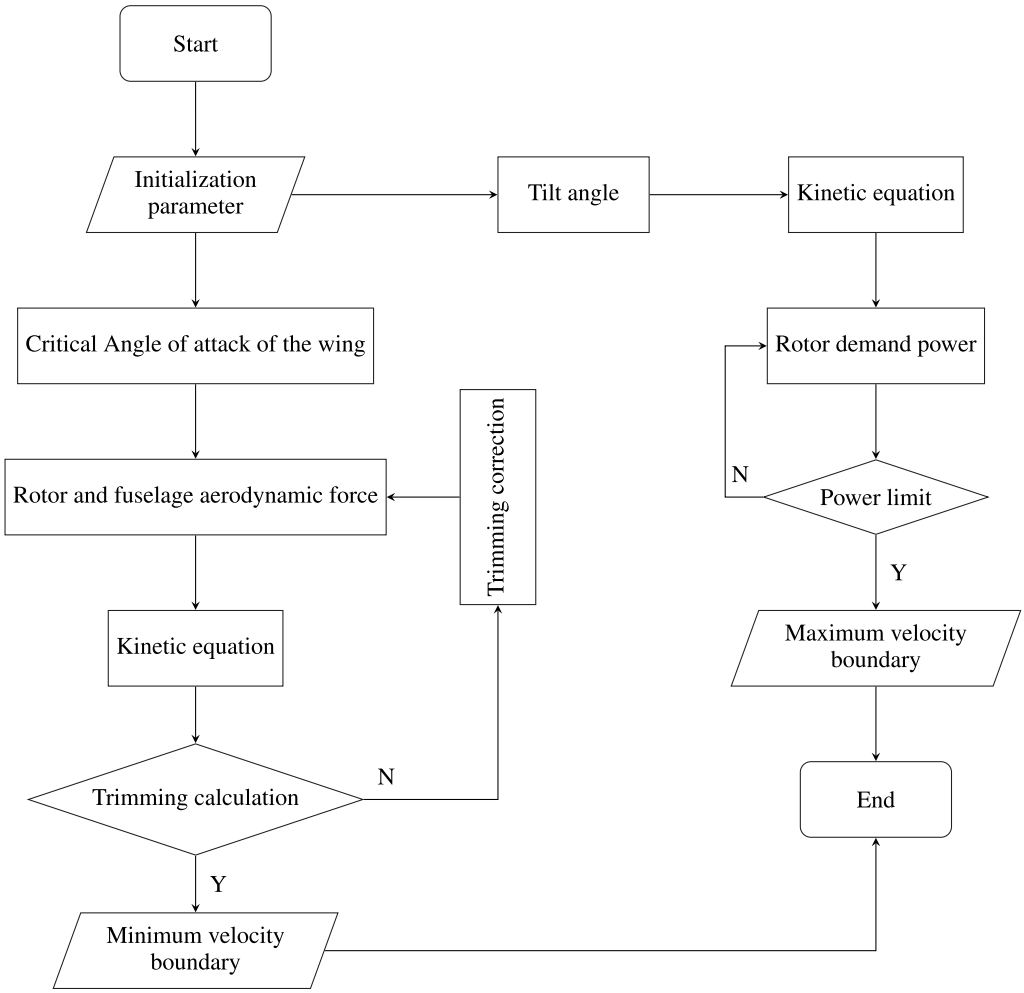

FIGURE 5. Conversion corridor calculation process.

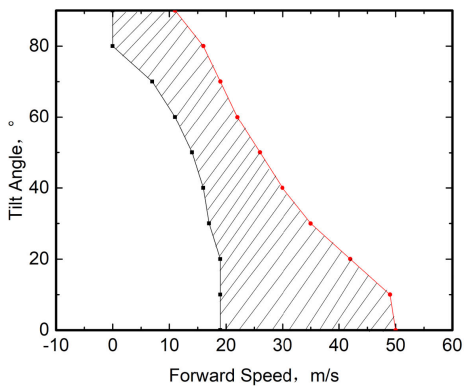

FIGURE 6. The conversion corridor of quad tilt rotor.

from the Figure 6 that the nacelle can be tilted forward by a maximum of 10° in helicopter mode, and the minimum flight speed when tilting to fixed-wing mode is $18m/s$, and the maximum flight speed is $50m/s$. The conversion of the aircraft is a variable speed and structure change process, and the maneuvering and distribution between the propeller and the wing must be reasonably controlled. If the forward speed is too low in fixed-wing mode, the wing will stall. Therefore, the conversion mode is a process related to altitude, forward speed, and tilt angle.

IV. MANIPULATION STRATEGY

A. MANIPULATION ALLOCATION

It is very important to manipulate the altitude and attitude to ensure the safety of the QTR in the conversion process. The altitude control and manipulation distribution strategy used in the QTR are shown in Table 2 and Figure 7.

It can be seen from Table 2 that the biggest difference between the manipulation allocation strategy used in this paper and the traditional manipulation allocation strategy is that the tilt angle is used to control the longitudinal channel in helicopter mode and the rotor is used to control the heading channel in fixed-wing mode. Using the tilt angle to control the longitudinal channel of the helicopter mode can keep the airframe at a positive angle of attack the wings can provide lift, and the nacelle can continue to tilt based on the current tilt angle when entering the conversion mode,

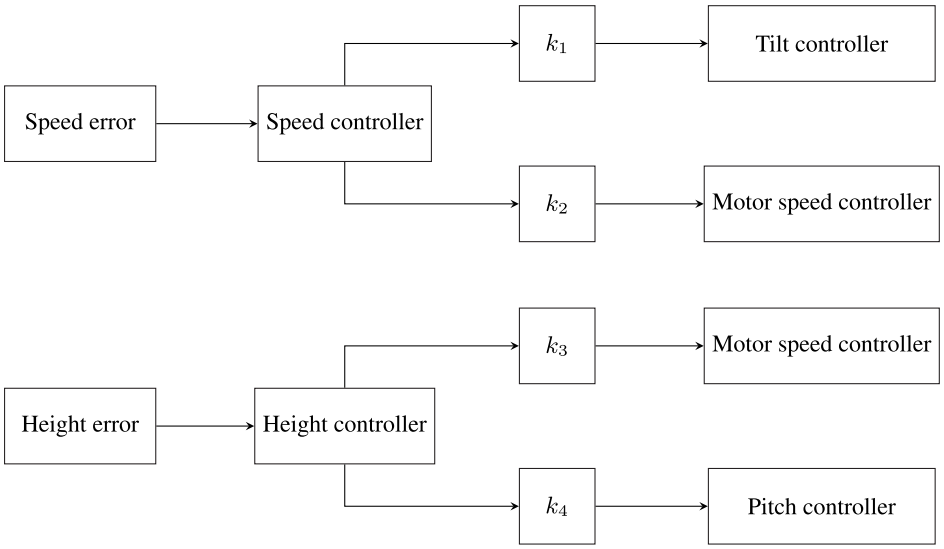

FIGURE 7. Manipulation distribution in conversion mode.

TABLE 2. Manipulation allocation of the QTR.

flight mode	channels	manipulation mechanism		
		tilt angle	rotor	control surface
helicopter	longitude	◯	◯	△
	latitude	△	◯	△
	course	△	◯	×
conversion	longitude	◯	◯	◯
	latitude	△	◯	◯
	course	△	◯	×
fixed-wing	longitude	△	△	◯
	latitude	△	△	◯
	course	△	◯	×

◯: use; △:selective use; ×: not use

which can effectively shorten the conversion time. Since the QTR designed in this paper does not have rudder, the pull generated by the rotor is still used in the fixed-wing mode to realize the heading channel control of the QTR. In Figure 7, the distribution coefficient k_1, k_2, k_3, k_4 are related to the tilt angle β_m and forward velocity V from figure 6.

$$k_1 = \left(\left(\cos\left(2\left(\pi/2 - \beta_m\right)\right)\right) + 1\right)/2 \tag{23}$$

$$k_2 = \left(\left(\sin\left(2\left(\pi/2 - \beta_m\right) - \pi/2\right)\right) + 1\right)/2 \tag{24}$$

$$k_3 = \begin{cases} 1, & u < 18 \\ 1 - \dfrac{u-18}{20}, & 18 \le u < 38 \\ 0, & u \ge 38 \end{cases} \tag{25}$$

$$k_4 = \begin{cases} 0, & u < 18 \\ \dfrac{u-18}{20}, & 18 \le u < 38 \\ 1, & u \ge 38 \end{cases} \tag{26}$$

where, the value 18 and 38 in the above equations are the minimum velocity of fixed-wing mode and the maximum velocity of conversion mode with $\beta_m = 60°$.

B. DIGITAL SIMULATION VERIFICATION RESULTS

In order to compare the manipulation strategy, we designed another three conversion strategies [32]. The conversion parameters of the four conditions are shown in table 3.

- **Condition 1:** conversion with different tilt rate, and waiting for the forward velocity to reach the set speed at the set tilt angle;
- **Condition 2:** directly conversion from helicopter mode to fixed wing mode at different tilt rate;
- **Condition 3:** conversion with one tilt rate, and waiting for the forward velocity to reach the set speed at the set tilt angle;
- **Condition 4:** directly conversion from helicopter mode to fixed wing mode at one tilt rate.

The simulation results are shown in Table 4 and Figure 8. It can be seen from the Figure 8 and Table 4 that when $\beta_m < 30°$, the simulation results are same due to the same of the four conditions. When tilt angle is small, the velocity of the vehicle is established too slow, according to the manipulation strategy, the vehicle will lower its head to increase the velocity which will lead to a reduction in altitude. When $30° \le \beta_m < 50°$, the nacelle of condition 2 and 4 continue tilting, and the nacelle of condition 1 and 3 will wait the velocity reaching 17.9 m/s at $\beta_m = 30°$. The velocity in condition 2 is increasing faster than it in condition4 due to the tilt rate of condition 2 is much faster. The lift increased by wing can not balance the vertical tension reduced by propeller, which will lead to the altitude reduced and the pitch angle became bigger to reduce the change of altitude. When the velocity reaches the set speed at $\beta_m = 30°$, the simulation results are all the same in the four conditions. In the conversion process, the change of altitude is crucial to the safety. From Figure 8 and Table 4, we can see that the most desired flight condition is condition 1, which has the shortest conversion time.

TABLE 3. Parameters of the four conditions.

	Condition1	Condition2	Condition3	Condition4
Tilt rate 1(°/s)	10	10	10	10
Tilt rate 2(°/s)	20	20	10	10
Tilt rate 3(°/s)	40	40	10	10
Set speed 1(m/s)	17.9④	—	17.9	—
Set speed 2(m/s)	20⑤	—	20	—
Set tilt angle 1(°)	30	—	30	—
Set tilt angle 2(°)	50	—	50	—

④,⑤ values are set according to figure 6

TABLE 4. Performance of the four conditions.

	Condition1	Condition2	Condition3	Condition4
Forward speed(m/s)	24.0	20.0	22.0	30.0
Minimum altitude(m)	-1.3	3.1	-5.5	-1.6
Pitch angle(°)	-3.0	4.5	0.4	8.3
Tilting time(s)	5.1	7.5	8.7	11.1

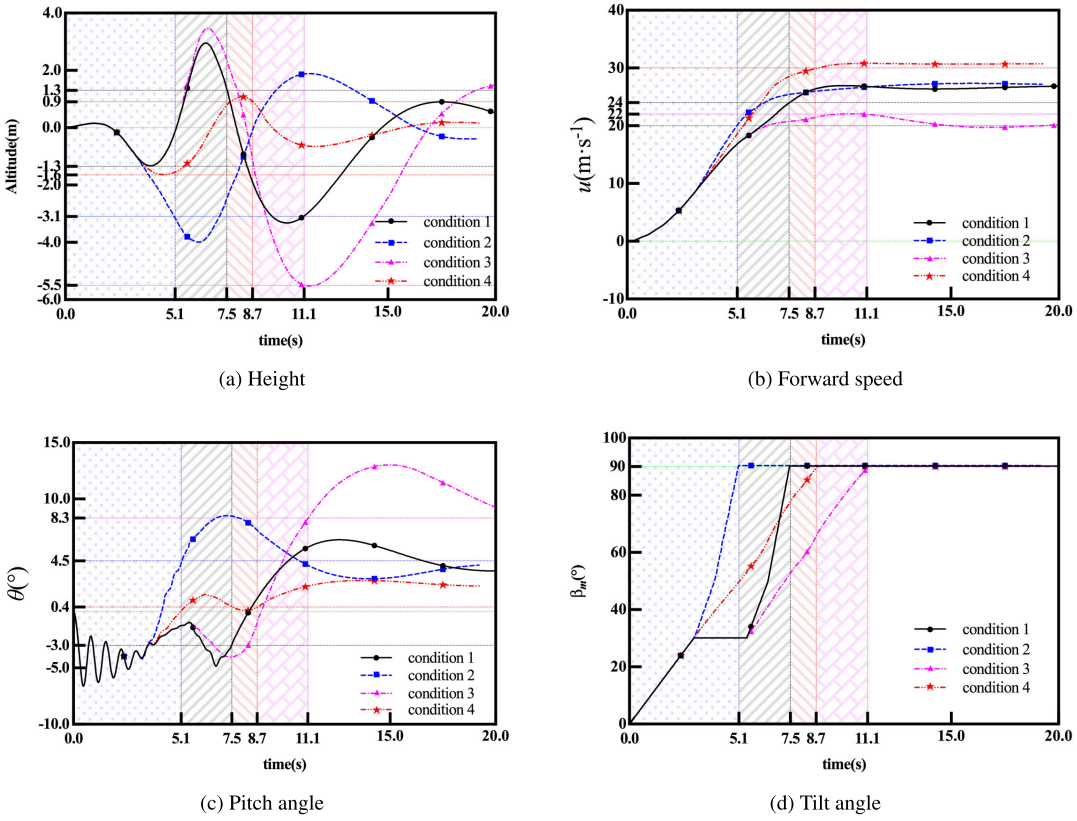

(a) Height

(b) Forward speed

(c) Pitch angle

(d) Tilt angle

FIGURE 8. Curves of flight simulation results.

The tilting path under the four conditions are shown in Figure 9. From this figure we can see that the tilting path of condition 2 is all out of the conversion corridor. The tilting path of condition 1 and condition 3 are similar in the conversion corridor. However, it can be seen that compared with figure 8, the altitude and pitch angle changing in condition 1 is smaller than it in condition 3.

V. FLIGHT CONTROL LAW

ADRC consists of three parts: Tracking Differentiator (TD), Extended State Observer (ESO) and Nonlinear State Error Feedback (NLSEF). The ADRC can observe and compensate for unknown disturbances [21], [33], [34]. Figure 10 shows the control law of ADRC.

A. TD

The input signal can arranged a transition process by TD [35] and obtained a differential signal:

$$\begin{cases} r_1(k+1) = r_1(k) + hr_2(k) \\ r_2(k+1) = r_2(k) \\ \qquad\qquad +h\text{fst}\left(r_1(k) - v(k), r_2(k), \delta, h\right) \end{cases} \tag{27}$$

TABLE 5. Key parameters in ADRC.

	parameters	initial value	description
TD	δ	10	Tracking speed
	h	0.001	Step size
ESO	β_1	50	Position tracking parameter of ESO
	β_2	675	Speed tracking parameter of ESO
	β_3	3375	Disturbance tracking parameter of ESO
	α_1	0.5	Parameter of saturation function
	α_2	0.25	Parameter of saturation function
	δ_1	0.0025	Error rate of saturation function
NLSEF	β_{01}	350	Nonlinear state feedback controller parameters k_p
	β_{02}	180	Nonlinear state feedback controller parameters k_d
	α_{01}	3/4	Nonlinear state feedback controller parameters $0 < \alpha_{01} < 1 < \alpha_{02}$
	α_{02}	3/2	Nonlinear state feedback controller parameters $0 < \alpha_{01} < 1 < \alpha_{02}$

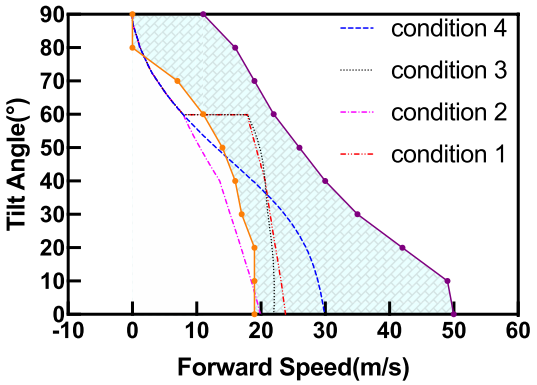

FIGURE 9. Tilting path of the four conditions.

$$\mathrm{fst}(x_1, x_2, \delta, h) = -\begin{cases} \delta \mathrm{sign}(a), & |a| > d \\ \delta \dfrac{a}{d}, & |a| \le d \end{cases} \tag{28}$$

$$a = \begin{cases} x_2 + \dfrac{a_0 - d}{2} \mathrm{sign}(y), & |y| > d_0 \\ x_2 + \dfrac{y}{h}, & |y| \le d_0 \end{cases} \tag{29}$$

$$\begin{cases} d = \delta h \\ d_0 = hd \\ y = x_1 + hx_2 \\ a_0 = \sqrt{d^2 + 8\delta|y|} \end{cases} \tag{30}$$

where, $r_1(k)$ and $r_2(k)$ are the tracking signals of $v(k)$ and $\dot{v}(k)$, δ is the tracking speed factor, h is the tracking step size.

B. EXTENDED SATE OBSERVER

The disturbance of the system can be estimated and compensated by the ESO [35]:

$$\begin{cases} e = z_1 - y \\ \dot{z}_1 = z_2 - \beta_1 e \\ \dot{z}_2 = z_3 - \beta_2 fal\,(e, \alpha_1, \delta) + bu \\ \dot{z}_3 = -\beta_3 fal\,(e, \alpha_2, \delta) \end{cases} \tag{31}$$

$$\mathrm{fal}(e, \alpha, \delta) = \begin{cases} \dfrac{e}{\delta^{1-\alpha}}, & |e| \le \delta \\ |e|^{\alpha} \mathrm{sign}(e), & |e| > \delta \end{cases} \tag{32}$$

where, $\beta_i > 0\,(i = 1, 2, 3)$, and $\alpha_1 = 0.5, \alpha_2 = 0.25$.

C. NONLINEAR STATE ERROR FEEDBACK

The structure of NLSEF [35] is shown below:

$$\begin{cases} e_1 = v_1 - z_1 \\ e_2 = v_2 - z_2 \\ u = \beta_1 \mathrm{fal}(e_1, \alpha_1, \delta) + \beta_2 \mathrm{fal}(e_2, \alpha_2, \delta) \end{cases} \tag{33}$$

where, $0 < \alpha_1 < 1 < \alpha_2$.

D. THE INFLUENCE OF ADRC PARAMETERS ON PERFORMANCE

The key parameters of ADRC are shown in Table 5. Fully understand the impact of each parameter on the performance of the controller, which has a certain effect on the parameter setting of ADRC. Therefore, this subsection takes the pitch channel of the QTR in the low-speed forward flight state as an example, and analyzes the impact of the key parameters of ADRC with the single parameter variable method. The input signal of the system is a unit step signal, and the disturbance signal in the system is a continuous disturbance signal of $1.2 \sin t$. The simulation results are shown in Figure 11 – Figure 13.

It can be seen from Figure 11(a) that the simulation step size has a great impact on the accuracy of the simulation results. The smaller the step size, the higher the accuracy of the simulation results. The simulation step size has an obvious relationship with the simulation time. Therefore, when setting the step size parameter, the time cost of the simulation needs to be comprehensively considered. It can be seen from Figure 11(b) that the tracking speed has a greater impact on the performance of the controller. As the tracking speed increases, the adjustment time of the system decreases, but at the same time the overshoot of the system will also increase. After increasing to a certain value, the adjustment time decreases less.

Figure 12 shows the influence curves of NLSEF key parameters on the system. It can be seen from Figure 12(a) and Figure 12(b) that the saturation function parameters in NLSEF have different control effects from those in ESO. As the parameter α_{01} increases, the overshoot of the system decreases, but at the same time, the system rise time becomes larger; as the parameter α_{02} increases, the system's ability to

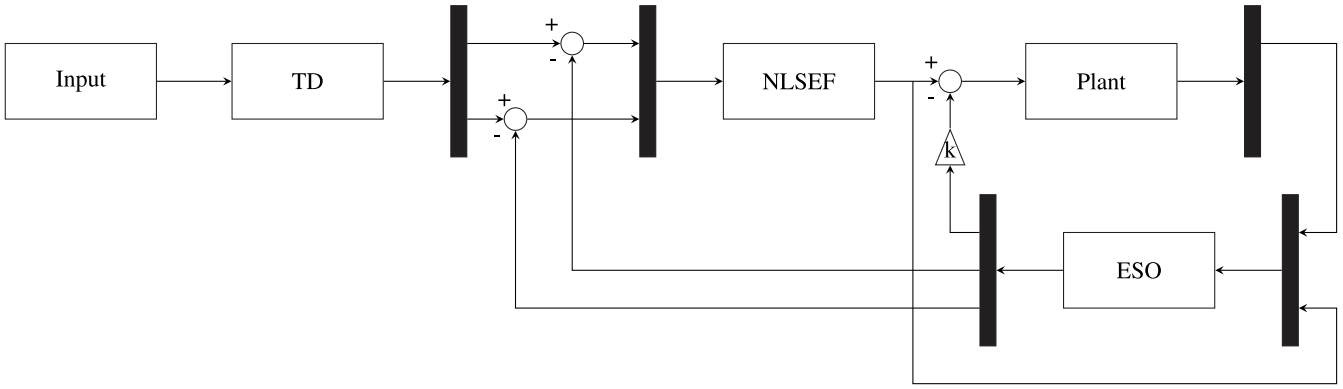

FIGURE 10. The structure of ADRC.

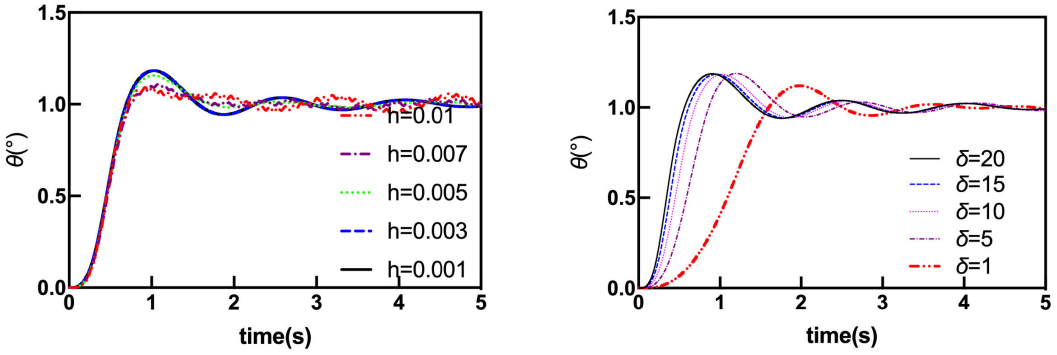

(a) h (b) δ

FIGURE 11. Key parameter influence curves in TD.

suppress signal jitter decreases. Figure 12(c) and Figure 12(d) are the controller parameters β_{01} and β_{02}, namely k_p and k_d in the PID controller parameters. The influence of this parameter is the same as that of the PID controller. With the increase of β_{01}, the system overshoots becomes larger, the rise time becomes shorter, and the system becomes oscillating; with the increase of β_{02}, the rise time of the system increases, but at the same time it has a restraining effect on the oscillation of the system.

Figure 13 is the curves of the influence of ESO key parameters on the controller performance. From Figure 13(a) and Figure 13(b), it can be seen that the saturation function parameter α_1 has a greater impact on the performance of the controller. As α_1 increases, the system's ability to suppress signal jitter becomes weaker. As α_2 increases, the system's performance of overshoot is reduced, but the ability to suppress signal jitter is also weakened. It can be seen from Figure 13(c) that when the value of the error accuracy parameter δ_1 is small, it basically has no effect on the control accuracy of the system. Figure 13(d), (e) and (f) are the main key parameters in the ESO. It can be seen from the Figure 13 that as the position tracking parameter β_1 increases, the overshoot of the system decreases, and the rise time becomes larger, the system oscillation weakens, but the system adjustment time is basically unchanged. With the increase of the speed tracking parameter β_2, the oscillation of the system is significantly improved. With the increase of the disturbance tracking parameter β_3, the anti-disturbance ability of the system is stronger.

It can be seen from the above analysis that in the process of adjusting ADRC parameters, within the acceptable range of time cost, in order to increase the accuracy of the simulation, the simulation step size h can be reduced as much as possible, and the tracking speed δ in TD can be increased; The saturation function parameters α_1, α_2, α_{01}, α_{02} and the error precision parameter δ_1 should be as small as possible within an appropriate range. ESO parameter β_1 should be as small as possible within the appropriate range, and β_2 and β_3 should be as large as possible within the appropriate range. NLSEF parameters β_{01} and β_{02} can be adjusted according to the classic PID control parameters.

VI. PROTOTYPE FLIGHT TEST VERIFICATION RESULTS

In order to verify the effectiveness and feasibility of the manipulation strategy for the QTR in this paper, this section conducts a flight test verification analysis. In order to ensure that the flight test verification can be carried out smoothly and safely, first established a 3D model of a QTR based

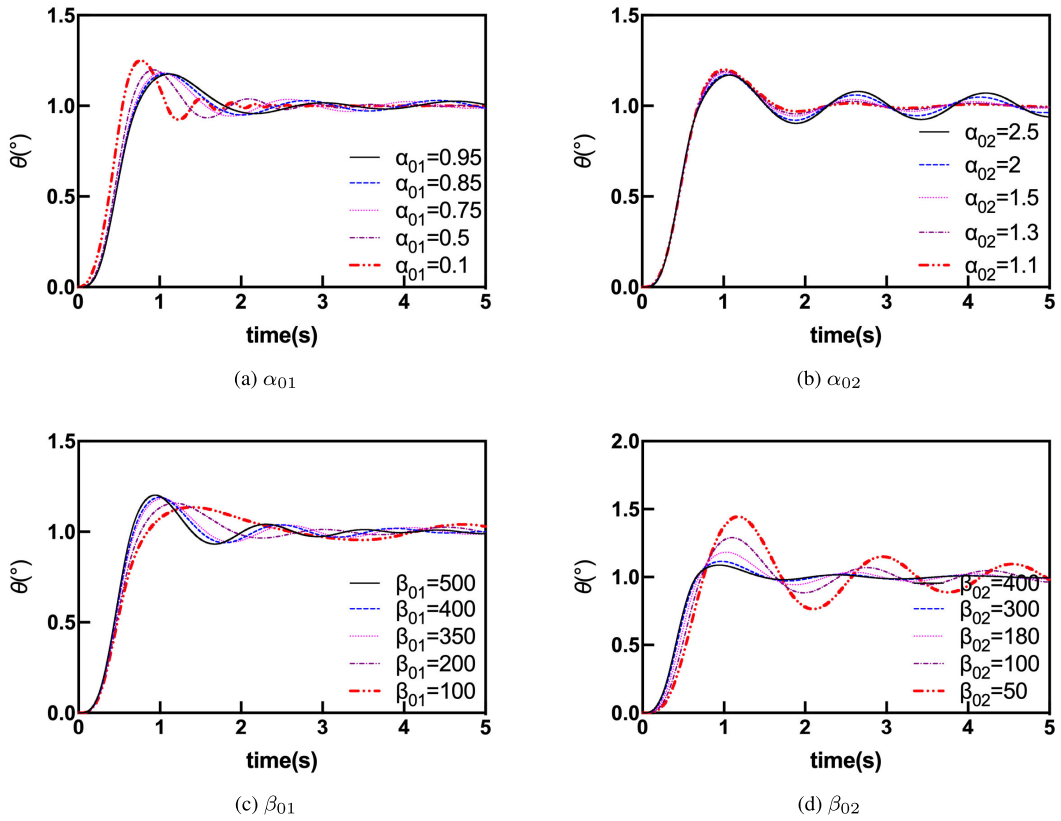

(a) α_{01} (b) α_{02}

(c) β_{01} (d) β_{02}

FIGURE 12. Key parameter influence curves in NLSEF.

on FlightGeaer, and carried out a 3D real scene simulation experiment based on Ardupilot and FlightGear. Finally, the flight test of the QTR UAV was completed to verify the effectiveness of the manipulation strategy. First, the nacelle is not tilted in the helicopter mode, and the position movement of the helicopter mode is realized only by the rotation speed of the rotor, to verify the effectiveness of the manipulation strategy and flight control law for QTR UAV with different take off weights. The pitch angle of the fuselage is negative during the forward flight, and the wings provide negative lift. Therefore, by tilting the nacelle to realize the position movement in the helicopter mode, it can ensure that the pitch angle of the fuselage is positive when flying in the helicopter mode, and the wings can provide a certain lift. Since the prototype aircraft does not have a rudder, the rotation speed of the rotor needs to be used to realize the heading control in fixed-wing mode. Figure 14 shows the test verification process.

A. 3D REAL SCENE SIMULATION

In order to reduce the development of the simulation model, the 3D model of QTR used in this paper is secondary development based on the existing V22 model in FlightGear, and its appearance is changed to a QTR model.

1) 3D MODEL DESIGN OF QTR UAV

In FlightGear, the creation of a new aircraft can be roughly divided into four steps: create the 3D model of the aircraft, create the flight dynamics model of the aircraft, create the animation and the operation of the aircraft, and realize each subsystem of the aircraft. Specifically, it can be divided into two major development areas: flight dynamics model development and aircraft 3D model development.

Through OpenSceneGraph technology, FlightGear supports various 3D file formats, including VRML1, AC3D, DXF, etc. Among them, .ac file is the standard used in most FG models. The model development in this paper also uses AC3D for secondary development.

Figure 15 is the rendering of the quad tilt rotor model developed with AC3D software. During modeling, it is important to note that the definition of the object name corresponds to the name in the configuration file below. The property "/sim/-model/path" in the main FlightGear property tree controls which models will be loaded. The easiest way to load a new model is to use the "-- prop" command:

```
1  fgfs --prop:/sim/model/path=Models/V44.ac
```

If set the 3D model to the default value for the aircraft instead of specifying it on the command line, it is needed to edit the aircraft configuration file. When starting FlightGear with the "--aircraft" option, it reads properties from one of the folders, such as:

```
1  fgfs --aircraft=v44
```

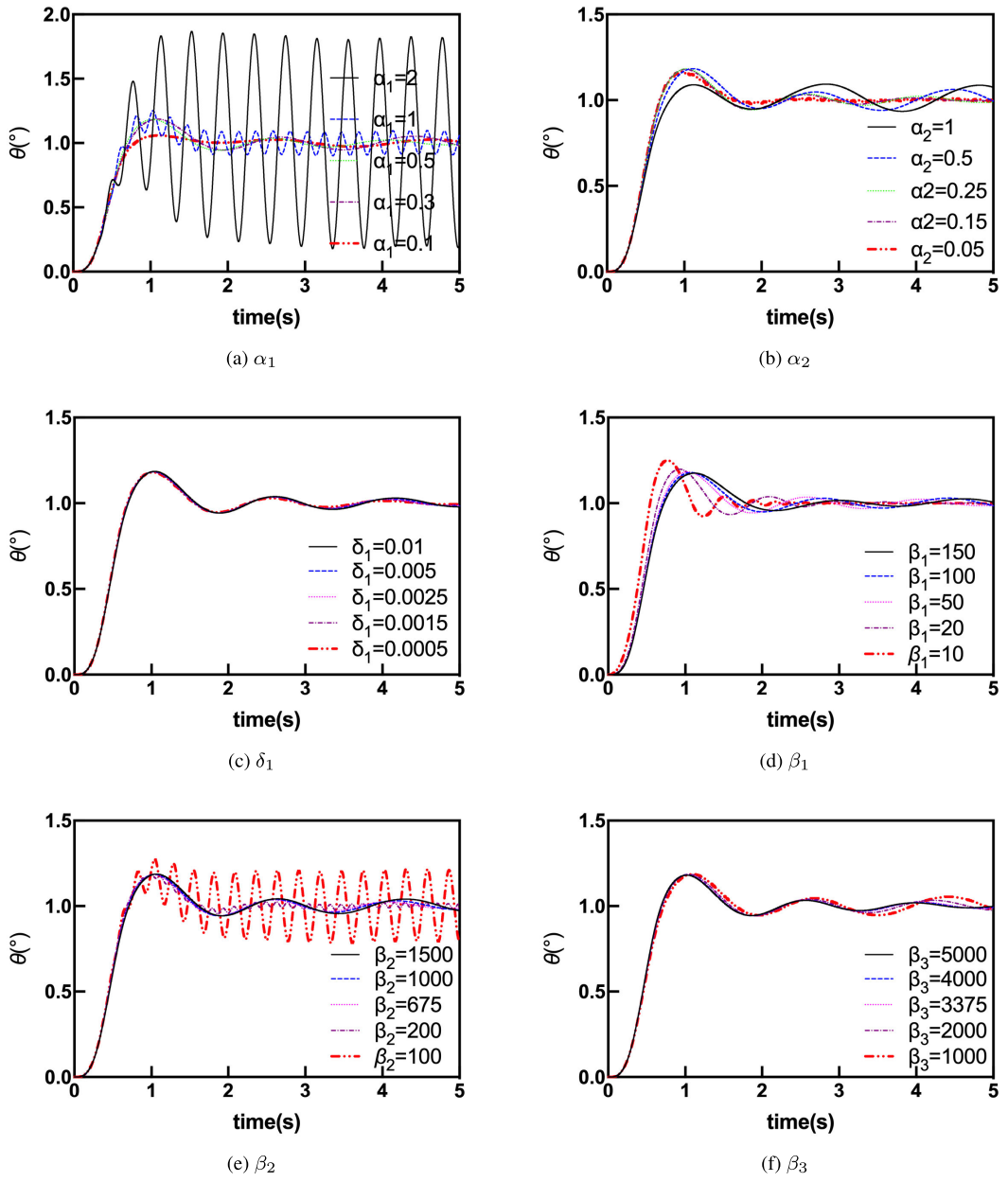

(a) α_1 (b) α_2 (c) δ_1 (d) β_1 (e) β_2 (f) β_3

FIGURE 13. Key parameter influence curves in ESO.

2) SIMULATION RESULT ANALYSIS

In the process of simulation, first to takeoff in helicopter mode, then set a target, let the QTR fly to the target point automatically. In the process of flight, if the current flight speed reached the set value, the flight mode automatically from helicopter turn to fixed-wing. When the QTR reaches the target point, it will hover around the target position. Then the flight path planning is carried out for the QTR. The QTR flies following the set trajectory in fixed-wing mode and land in helicopter mode. Figure 16 shows the flight modes of QTR during the whole flight. In the whole simulation process, the QTR can follow the commands very well, and through the 3D real scene simulation, the nacelle state of the QTR during the conversion mode and the flight state of the QTR can be better reflected.

B. FLIGHT IN HELICOPTER MODE WITHOUT NACELLE TILTING

1) HOVERING

It can be seen from Figure 18 and Figure 19 that the attitude of the QTR UAV can well follow the input of the control, and the aircraft can well maintain the stability of the attitude in the process of flight, and the change of the attitude angle is kept within a small angle. In Figure 20, you can see the course

FIGURE 14. Flight test verification process.

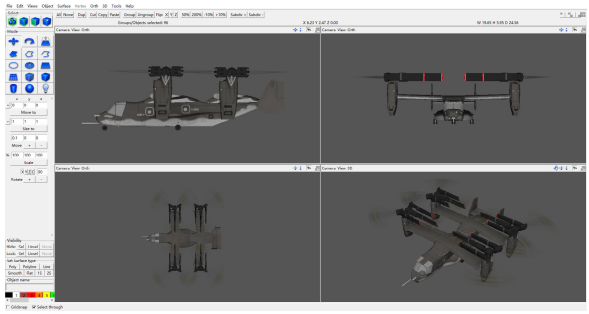

FIGURE 15. 3D model of QTR.

angle control has a certain delay, the effect of the following is not as obvious as pitch and roll channels. Through the hover flight test of the QTR UAV, it can be seen from the flight test results that in the stabilization mode the attitude and position stabilization can be controlled during the entire flight of the UAV, and the response of each channel can be follow up the manipulation input very quickly. The response error of each channel is within the allowable range, which is consistent with the simulation results of the control law. It can be seen that it has a good control effect which able to achieve the expected flight control results.

2) FIXED ALTITUDE AND FIXED POINT

It can be seen from the Figure 21 that in the stabilization mode, when the QTR is moving in a horizontal position, the altitude will change to a certain extent. This is because when the throttle is constant, the aircraft is in the process of horizontal movement, the attitude of the aircraft changes to a certain angle, and the rotor will provide a force component on the horizontal plane, resulting in a change in the magnitude

(a) Helicopter mode

(b) Conversion mode

(c) Fixed wing mode

(d) Landing

FIGURE 16. Flight modes of QTR in 3D simulation.

FIGURE 17. Hovering flight verification.

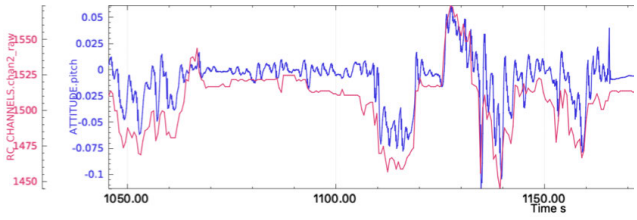

FIGURE 18. Pitch channel input and output comparison.

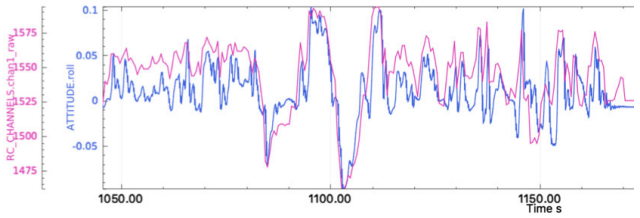

FIGURE 19. Roll channel input and output comparison.

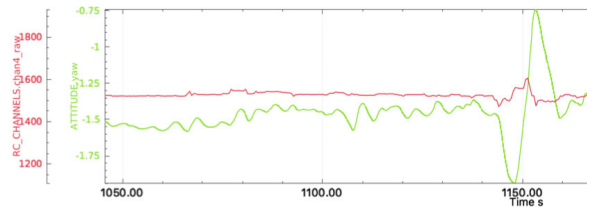

FIGURE 20. Yaw channel input and output comparison.

of the force in the vertical direction, and thus the height of the aircraft will change to a certain extent. However, in the fixed altitude and fixed point modes, when the aircraft is moved horizontally, the aircraft will automatically adjust the motor speed to maintain a stable altitude. In the fixed altitude mode, the aircraft can keep the position unchanged when the control amount is not given. When moving forward, backward, left, right and yaw control, the aircraft will perform corresponding response movements while maintaining the same height. When the throttle is manipulated, the aircraft only changes in altitude, and the aircraft's attitude is always stable. In the fixed point mode, the aircraft can hover steadily without major drift. According to the data analysis of the UAV's fixed altitude and fixed point, it can be seen that the design of the control law can realize the fixed altitude and fixed point control of the TQR UAV.

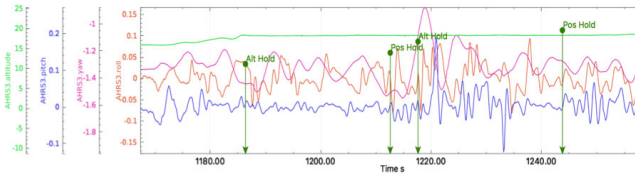

FIGURE 21. Altitude and attitude changes with the flight mode switch.

C. FULL MODAL FLIGHT WITH NACELLE TILTING

The flight data is analyzed in detail during the flight test. The specific flight mode can be divided into the following six parts: vertical takeoff, altitude climb, forward conversion, fixed-wing cruise, backward conversion, vertical landing.

1) VERTICAL TAKEOFF

After the ground checks and tests before the flight test are all completed, the UAV takes off in helicopter mode, and its flight data is shown in Figure 22 - 24.

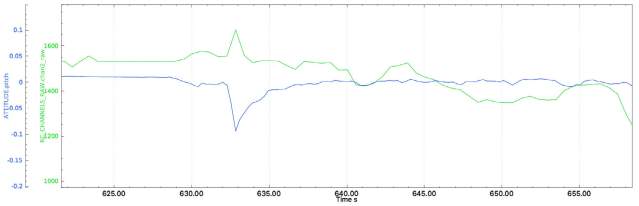

FIGURE 22. Pitch channel input and output comparison.

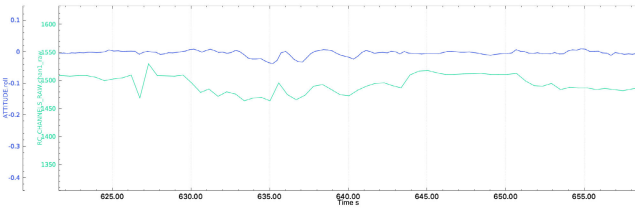

FIGURE 23. Roll channel input and output comparison.

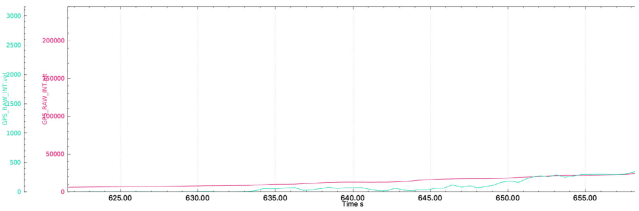

FIGURE 24. Altitude channel input and output comparison.

It can be seen from the Figure 22 that in the hovering mode, the pitch angle of the UAV remains basically unchanged at around 0°, and the controlled pitch channel is mapped to the nacelle tilting angle in the helicopter mode. Therefore, the pitch angle does not change with the pitch control. Figure 23 shows the relationship between the roll angle and the manipulation input. It can be seen from the figure that when the manipulation input is not given, the roll angle of the UAV basically remains unchanged, and the response characteristics of the manipulation input is better. During the whole hovering process, the attitude angle of the UAV basically did not change, and the stability of the UAV was better. When the throttle amount reaches 40%, the pulling force provided by the rotor is sufficient to make the UAV take off. The altitude can be well stabilized at the given throttle amount.

2) ALTITUDE CLIMB

After the QTR is taking off, in order to carry out a safe conversion flight, the QTR needs to be raised to a certain atitude. The specific attitude information during the altitude climb is shown in the Figure 25– 27:

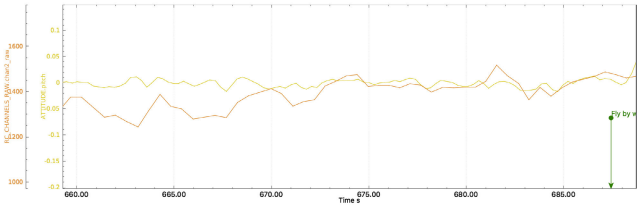

FIGURE 25. Pitch channel input and output comparison.

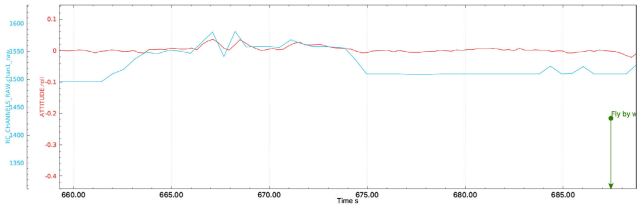

FIGURE 26. Roll channel input and output comparison.

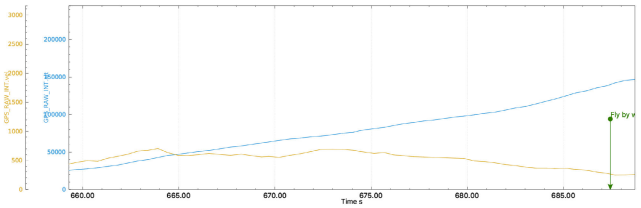

FIGURE 27. Altitude and velocity.

When the given throttle amount continues to increase (more than 40%), the rotor provides sufficient pulling force to raise the QTR UAV. During this process, the attitude angle of the UAV basically did not change and remained stable within a certain value. The forward flight speed has a small range change. This is because in the helicopter mode, the pitch channel corresponds to the tilt of the nacelle. The pitch control causes the nacelle to tilt, so that the UAV gains a certain forward pulling force.

3) FORWARD CONVERSION

In the entire flight process, forward conversion is the most important flight mode. When the altitude rises to a certain level (more than 50m), the nacelle starts to tilt forward at a fixed speed (15°/s), when the tilt angle reaches 60°, If the forward speed is greater than the set speed of $18m/s$, the nacelle will continue to tilt to 90°, otherwise the nacelle will wait for the speed to reach the set speed at the position of 60°.

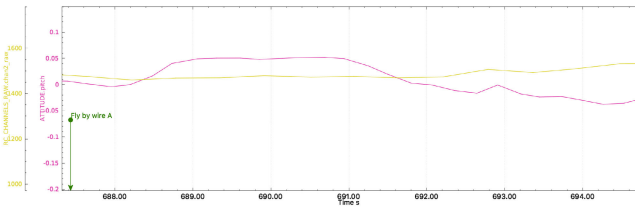

FIGURE 28. Pitch channel input and output comparison.

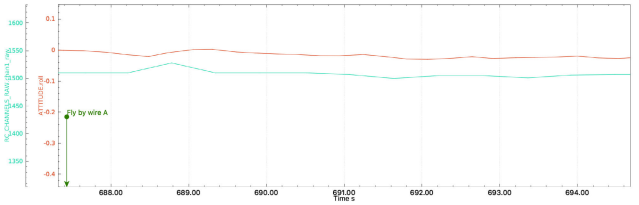

FIGURE 29. Roll channel input and output comparison.

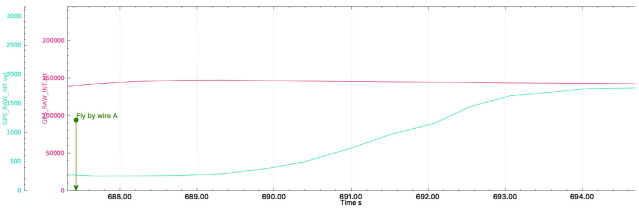

FIGURE 30. Altitude and velocity.

During the entire tilting process, there is no input for the control of the pitch angle. However, in the transition phase, in order to ensure the safe transition of the UAV, and to control the altitude, it is necessary to simultaneously change the motor speed and the attitude angle of the fuselage to stabilize the altitude. From the Figure 28 and 29, it can be seen that the pitch angle has basically not changed. During the entire tilting process, there is no operation input for the roll angle, and the roll angle of the UAV remains basically unchanged during the entire process, and the UAV has better stability enhancement effects. It can be seen from the Figure 30 that the height of the UAV remains basically unchanged during the entire tilting process. However, at the beginning of the transition, the nacelle's tilting rate is slow and the forward flight speed is established slowly. When the tilt angle becomes larger, the speed will increase rapidly. When the current flying speed reaches the set speed of $18m/s$, the nacelle will pass the set angle of 60° smoothly, reach the horizontal position, and complete the modal transition in $6s$.

4) FIXED-WING CRUISE

When the nacelle is fully tilted to the horizontal position, the UAV starts to fly in fixed-wing mode, and its cruise data results are shown in Figure 31 – Figure 34:

From Figure 31 and Figure 32, it can be seen that in the cruise mode, the attitude of the UAV can follow the control input well, and it has certain stabilization characteristics. Since the UAV has no rudder, so the heading control is realized by the differential speed of four motors. It can also be seen from the Figure 33 that the motor differential speed can effectively control the heading of the UAV. In the heading control, the yaw angular velocity is controlled. From the Figure 34, it can be seen that the altitude of the QTR remains basically unchanged during the entire cruise, but the forward flight speed changes greatly.

5) BACKWARD CONVERSION

After the fixed-wing cruise flight is about 1 minute, the QTR changes from fixed-wing mode to helicopter mode and prepare to vertical landing. During the conversion of the nacelle backward tilt, the nacelle's tilting speed is a fixed rate ($15°/s$), and the nacelle reaches the vertical position after $6s$, which completing the transition from fixed-wing mode to helicopter mode. During the transition process of the backward conversion, no control input was given to the QTR. QTR automatically complete the entire tilting process. The information of its attitude, altitude and forward speed is shown in the Figure 35 – Figure 37.

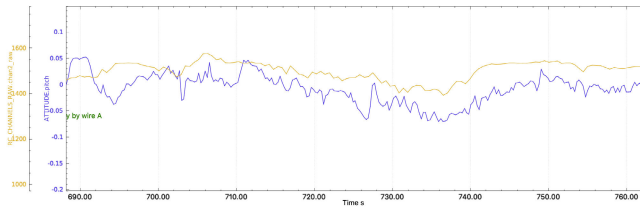

FIGURE 31. Pitch channel input and output comparison.

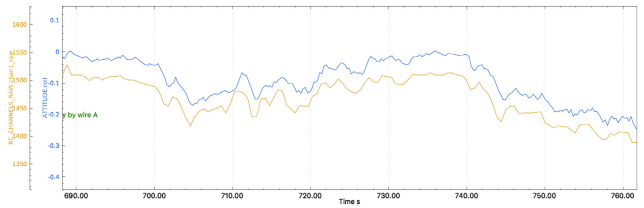

FIGURE 32. Roll channel input and output comparison.

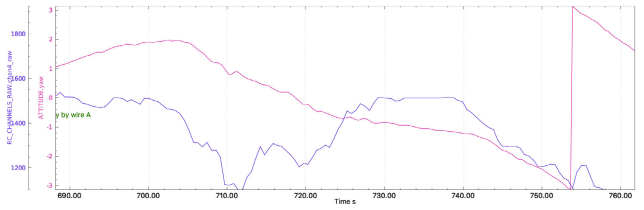

FIGURE 33. Yaw channel input and output comparison.

From the Figure 35 and Figure 36, it can be seen that the pitch and roll angles of the QTR remain basically unchanged and stay near 0° during the entire backward conversion process. The QTR has a good stability enhancement characteristics. It can be seen from the Figure 37 that after the start of the tilt, the forward flight speed will drop rapidly. When the nacelle tilt angle is large, the speed will drop slowly, and it

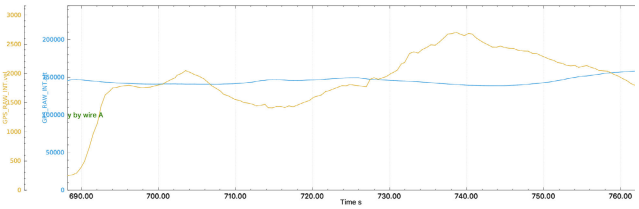

FIGURE 34. Altitude and velocity.

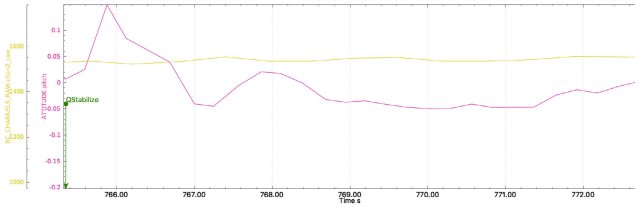

FIGURE 35. Pitch channel input and output comparison.

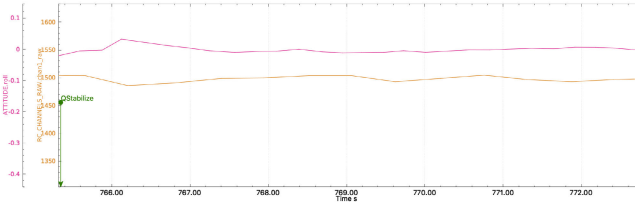

FIGURE 36. Roll channel input and output comparison.

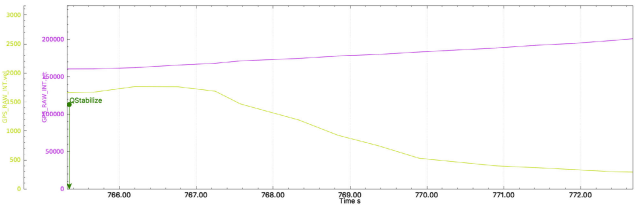

FIGURE 37. Altitude and velocity.

will eventually be $0m/s$. This is because the forward pulling force of the rotor will become smaller with the nacelle tilts, and the lift provided by the wing of the UAV will gradually transfer to the pulling force of the rotor. It can also be seen from the figure that the height of the QTR will increase during the entire backward conversion. This is because, at the beginning of the backward conversion, the forward flight speed of the UAV is relatively high, and the lift provided by the wings is sufficient. The rotor provides an upward pulling force, so that the pulling force of the rotor and the lift provided by the wings are greater than the gravity of the QTR, so that the QTR will increase when it tilts backward.

6) VERTICAL LANDING

When the nacelle fully tilts from the horizontal position to the vertical position after $6s$, the QTR UAV changes to helicopter mode and starts flying in the helicopter mode. In this mode, the controlled pitch channel is mapped to the nacelle tilt angle. The pitch angle of the fuselage is set to 0°. In the process of vertical landing, its attitude, altitude and forward speed information are shown in Figure 38 – Figure 40.

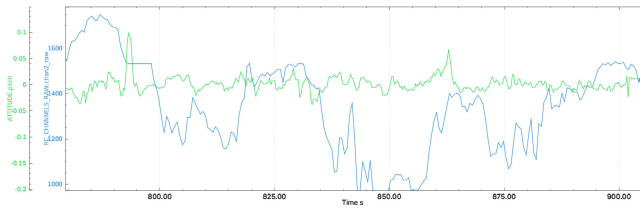

FIGURE 38. Pitch channel input and output comparison.

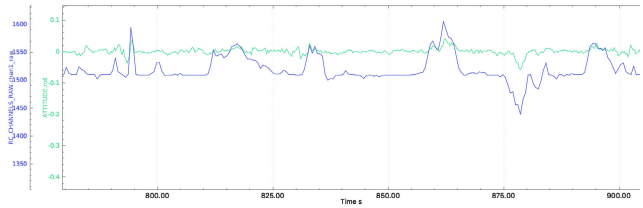

FIGURE 39. Roll channel input and output comparison.

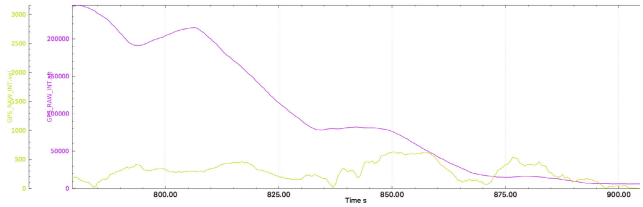

FIGURE 40. Altitude and velocity.

It can be seen from the figure 38 that when flying with a helicopter mode, the pitch angle of the fuselage remains basically unchanged during the whole vertical landing process, basically maintaining around 0°. The pitch control corresponds to the tilt angle of the nacelle, which causes a change in the forward flight speed in the Figure 40, and moves the horizontal position. Figure 39 describes the response relationship between the roll angle and the manipulation input during vertical landing. It can be seen from the figure that the roll angle of the UAV can quickly follow the manipulation input. It can be seen from the altitude information in Figure 40. When the conversion is complete, decrease the input of the throttle, the altitude of the drone will decrease, and finally land.

D. DISCUSSION

The partial flight path of the prototype QTR flight test is shown in Figure 41. Figure 42 shows several key modal states of the prototype aircraft during the flight test. In hover mode, the UAV can maintain good stability and be sensitive to control. The acceleration process of the UAV is relatively obvious through the tilt of the nacelle and the acceleration is relatively fast. During the conversion, the nacelle began to tilt forward and the forward speed increased rapidly. When the current flight speed reaches 18m/s, the nacelle will continue to tilt to the horizontal position to complete the mode change and switch to the fixed-wing mode. Under the fixed-wing mode cruise flight, the unmanned vehicle can quickly follow the control of the remote control to conduct a stable stability control flight.

FIGURE 41. Partial flight path.

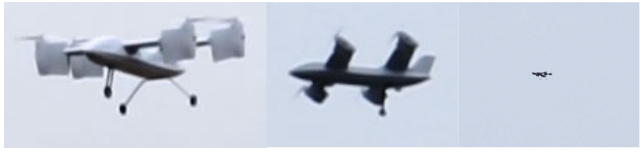

(a) hover (b) conversion (c) cruise

FIGURE 42. Prototype aircraft flight mode.

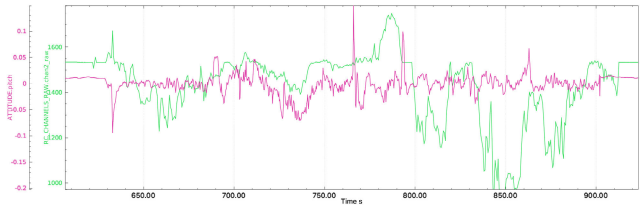

FIGURE 43. Pitch channel input and output comparison.

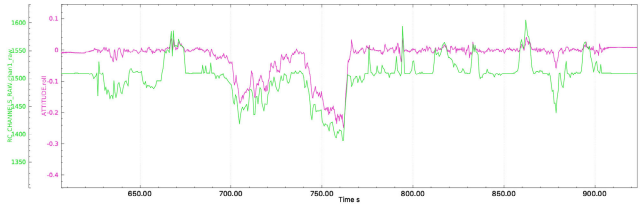

FIGURE 44. Roll channel input and output comparison.

Figure 43 shows the relationship between the pitch channel input of the prototype and the pitch angle of the UAV. In the helicopter mode, the UAV still uses the pitch channel manipulated to correspond to the tilt of the nacelle to keep the attitude stable. It can be seen from the figure that in the helicopter mode, the pitch angle of the fuselage basically remains unchanged, stable at 0°. When switched to fixed-wing mode, the pitch angle of the fuselage can quickly follow the control input. In the helicopter mode, the stabilization effect is more significant.

Figure 44 shows the result of the roll angle following manipulation input on the roll channel of the prototype QTR. As can be seen from the figure, the roll angle can quickly follow the control input in the helicopter and fixed-wing modes. In helicopter mode, the stabilization effect of the rolling channel is more significant.

Figure 45 shows the changes in altitude and forward speed during the entire flight. As can be seen from the figure, when the mode is changed from helicopter to fixed-wing, the forward speed will increase rapidly, and the altitude will remain basically unchanged. After the current flying speed reaches the required speed of the fixed-wing, the nacelle directly tilts to the horizontal position, and the UAV starts to fly in the fixed-wing mode. When the UAV changes from the fixed-wing mode to the helicopter mode, the forward flight speed begins to decrease, and the altitude rises. Because the forward flight speed is high, the lift provided by the wings is enough to offset the gravity of the fuselage, and the nacelle starts to tilt upwards, the rotor will generate additional pulling force on the fuselage, causing the QTR to rise.

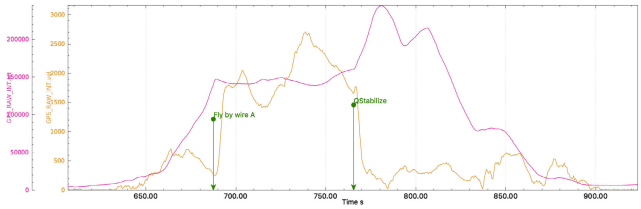

FIGURE 45. Altitude and velocity.

VII. CONCLUSION

In this paper, aiming at the complex conversion process of QTR. To solve the problem of redundancy and coupling in conversion mode, the conversion corridor of the QTR with partial tilt wing is established. The altitude, forward velocity and tilt angle are introduced into the manipulation strategy to ensure the stability of the altitude and attitude in conversion process. The tilt angle of nacelle is used to control the longitude of the QTR in helicopter mode and the speed error of propeller is used to control the course of QTR in fixed-wing mode. The simulation based on ADRC controller is carried out and the results show that the manipulation strategy can ensure the stability of the altitude and attitude of the QTR with partial tilt wing in the conversion process.

The flight tests show that it is effective to control the horizontal movement of the helicopter mode by the inclination of the nacelle and the course of the fixed-wing mode by the differential speed of the motors. It verifies that the manipulation strategy and allocation are reasonable and effective in the conversion mode.

ACKNOWLEDGMENT

The authors would like to express their gratitude to all those who have helped during the writing of this article.

DECLARATION OF CONFLICTING INTERESTS

The author(s) declared no potential conflicts of interest with respect to the research, authorship, and/or publication of this article.

REFERENCES

[1] Z. Wang and J. Li, "3D simulation of flight control system for quad tilt rotor UAV based on flightgear," *IOP Conf. Ser., Earth Environ. Sci.*, vol. 440, Mar. 2020, Art. no. 052056.
[2] Z. Wang and J. Li, "A novel active disturbance rejection control for the quad tilt rotor in conversion process," *IOP Conf. Ser., Earth Environ. Sci.*, vol. 440, Mar. 2020, Art. no. 032036.
[3] Z. Wang, H. Zhao, D. Duan, Y. Jiao, and J. Li, "Application of improved active disturbance rejection control algorithm in tilt quad rotor," *Chin. J. Aeronaut.*, vol. 33, no. 6, pp. 1–23, 2020.
[4] C. Papachristos, K. Alexis, and A. Tzes, "Hybrid model predictive flight mode conversion control of unmanned quad-TiltRotors," in *Proc. Eur. Control Conf. (ECC)*, Jul. 2013, pp. 1793–1798.
[5] C.-J. Kim, S. Sung, S. H. Park, S. N. Jung, and T. S. Park, "Numerical time-scale separation for rotorcraft nonlinear optimal control analyses," *J. Guid., Control, Dyn.*, vol. 37, no. 2, pp. 658–673, Mar. 2014.
[6] C. L. Bottasso, A. Croce, D. Leonello, and L. Riviello, "Optimization of critical trajectories for rotorcraft vehicles," *J. Amer. Helicopter Soc.*, vol. 50, no. 2, pp. 165–177, Apr. 2005.
[7] D. Chao, B. Huihui, and Z. Jianping, "Nonlinear stabilization control of tilt rotor UAV during transition flight based on HOSVD," in *Proc. IEEE Chin. Guid., Navigat. Control Conf. (CGNCC)*, Aug. 2016, pp. 154–159.
[8] P. Huangzhong, Z. Ziyang, and G. Chen, "Tiltrotor aircraft attitude control in conversion mode based on optimal preview control," in *Proc. IEEE Chin. Guid., Navigat. Control Conf.*, Aug. 2014, pp. 1544–1548.
[9] E. B. Carlson and Y. J. Zhao, "Prediction of tiltrotor height-velocity diagrams using optimal control theory," *J. Aircr.*, vol. 40, no. 5, pp. 896–905, Sep. 2003.
[10] Y. Okuno and K. Kawachi, "Optimal takeoff procedures for a transport category tiltrotor," *J. Aircr.*, vol. 30, no. 3, pp. 291–292, May 1993.
[11] G. Flores and R. Lozano, "Transition flight control of the quad-tilting rotor convertible MAV," in *Proc. Int. Conf. Unmanned Aircr. Syst. (ICUAS)*, May 2013, pp. 789–794.
[12] G. R. Flores-Colunga and R. Lozano-Leal, "A nonlinear control law for hover to level flight for the quad tilt-rotor UAV," *IFAC Proc. Volumes*, vol. 47, no. 3, pp. 11055–11059, 2014.
[13] A. Oosedo, S. Abiko, S. Narasaki, A. Kuno, A. Konno, and M. Uchiyama, "Large attitude change flight of a quad tilt rotor unmanned aerial vehicle," *Adv. Robot.*, vol. 30, no. 5, pp. 326–337, Mar. 2016.
[14] L. Haixu, Q. Xiangju, and W. Weijun, "Multi-body motion modeling and simulation for tilt rotor aircraft," *Chin. J. Aeronaut.*, vol. 23, no. 4, pp. 422–425, 2010.
[15] R. Zheng, Y. He, Z. Liu, L. Yang, and F. Gu, "Mode transition control of dual tilt rotor unmanned aerial vehicle based on dynamic analysis," in *Proc. Chin. Control Decis. Conf. (CCDC)*, Aug. 2020, pp. 1528–1533.
[16] Y. Sakai and S. Abiko, "Flight experiment for seamless 90-degree attitude transition flight of a quad tilt-rotor UAV," in *Proc. JSME Annu. Conf. Robot. Mechatronics (Robomec)*, 2020, pp. 2A2–B01.
[17] D. Wang, J. Guo, and H. Pu, "Rudder surface allocation and active disturbance rejection control in transition mode of unmanned tilt rotor aircraft," *Electro-Opt. Control*, vol. 26, no. 4, pp. 27–31, 2019.
[18] J. F. Pan, N. C. Cheung, and J. M. Yang, "Auto-disturbance rejection controller for novel planar switched reluctance motor," *IEE Proc.-Electr. Power Appl.*, vol. 153, no. 2, pp. 307–316, Mar. 2006.
[19] H. Huang, L. Wu, J. Han, G. Feng, and Y. Lin, "A new synthesis method for unit coordinated control system in thermal power plant-ADRC control scheme," in *Proc. Int. Conf. Power Syst. Technol.*, 2004, pp. 133–138.
[20] J. Su, W. Qiu, H. Ma, and P.-Y. Woo, "Calibration-free robotic eye-hand coordination based on an auto disturbance-rejection controller," *IEEE Trans. Robot.*, vol. 20, no. 5, pp. 899–907, Oct. 2004.
[21] Z. Yang, H. Rui, Y. Zhao, and H. Hu, "Design of an active disturbance rejection control for transonic flutter suppression," *J. Guid. Control Dyn.*, vol. 40, no. 1, pp. 1–12, 2017.
[22] F. Zhang and P. LU, "Analysis of tilting mode control and tilting strategy of tiltrotor," *Flying Missile*, vol. 11, pp. 54–56, Dec. 2016.
[23] F. Zhang, P. LU, T. Jiang, and F. Shi, "Research on transition mode manipulation strategy of tilting tri-rotor UAV based on fuzzy control," *Electro-Opt. control*, vol. 25, no. 238, pp. 36–40, 2018.
[24] Q. Xia, J. Xu, and K. Jin, "Modeling and maneuvering allocation strategy for tilt-rotor aircraft," *J. Aeronaut.*, vol. 28, no. 9, pp. 2016–2028, 2013.
[25] X. Yan and R. Chen, "Optimal control strategy of tilt rotor aircraft during dynamic tilt transition," *Acta Aeronautica Sinica*, vol. 38, no. 7, pp. 54–64, 2017.
[26] G. R. Flores, J. Escareño, R. Lozano, and S. Salazar, "Quad-tilting rotor convertible MAV: Modeling and real-time hover flight control," *J. Intell. Robot. Syst.*, vol. 65, nos. 1–4, pp. 457–471, Jan. 2012.
[27] Z. Wang, J. Li, and D. Duan, "Manipulation strategy of tilt quad rotor based on active disturbance rejection control," *Proc. Inst. Mech. Eng., G, J. Aerosp. Eng.*, vol. 234, no. 3, pp. 573–584, Mar. 2020.
[28] Z. G. Wang, D. Y. Duan, Y. W. Yang, H. R. Yu, and J. B. Li, "Analysis of flight dynamics characteristics of tilt quad rotor with partial tilt-wing," *Trans. Nanjing Univ. Aeronaut. Astronaut.*, vol. 36, no. 6, pp. 938–951, 2019.
[29] Z. Wang, R. Zu, D. Duan, and J. Li, "Tuning of ADRC for QTR in transition process based on NBPO hybrid algorithm," *IEEE Access*, vol. 7, pp. 177219–177240, 2019.
[30] W. Johnson, *Helicopter Theory*. Mineola, NY, USA: Dover, Mineola, 1980.
[31] A. Okan, O. Tekinalp, M. Kavsaoglu, O. Armutcuoglu, and E. Tulunay, "Flight mechanics analysis of a tilt-rotor UAV," in *Proc. AIAA J.*, vol. 99, Dec. 1999, p. 4255.
[32] Z. Lyu, Z. Wang, D. Duan, L. Lin, J. Li, Y. Yang, Y. Chen, and Y. Li, "Tilting path optimization of tilt quad rotor in conversion process based on ant colony optimization algorithm," *IEEE Access*, vol. 8, pp. 140777–140791, 2020.
[33] C. Lin, H. Wang, J. Yuan, and M. Fu, "An online path planning method based on hybrid quantum ant colony optimization for AUV," *Int. J. Robot. Autom.*, vol. 33, no. 4, pp. 435–444, 2018.
[34] D. Li and H. H. Liu, "Sensor bias fault detection and isolation in a large multirotor aerial vehicle using active disturbance rejection control," in *Proc. AIAA Inf. Syst.*, Jan. 2018, p. 249.
[35] J. Han, "From PID to active disturbance rejection control," *IEEE Trans. Ind. Electron.*, vol. 56, no. 3, pp. 900–906, Mar. 2009.

YONGHONG CHEN received the Ph.D. degree from the Shenyang Institute of Automation, Chinese Academy of Sciences. She currently works as a Vice Minister and a Chief Project Designer with Yangzhou Academy of Collaboration & Innovation Company Ltd. She is also a Senior Engineer. Her research interests include collaborative operations and integrated design of radio frequency systems.

ZHIGANG WANG received the B.Sc. degree in space science and technology and the M.Sc. degree in software engineering from the Harbin Institute of Technology, Harbin, China, in 2012 and 2014, respectively, and the Ph.D. degree in aerospace vehicle design from the Nanjing University of Aeronautics and Astronautics, Nanjing, China, in 2020. He currently works as an Engineer with Yangzhou Academy of Collaboration & Innovation Company Ltd. He is also an Engineer. His research interests include dynamic modeling and control of novel aircraft, intelligent optimization algorithm, navigation and obstacle avoidance of aircraft in denial environment, and cooperative control of swarm formation.

ZHICHAO LYU received the B.Sc. degree in optical fiber communications from the Chongqing University of Posts and Telecommunications, Chongqing, China, in 2012, and the M.Sc. degree in aerospace engineering from the Harbin Institute of Technology, Harbin, China, in 2015. From 2015 to 2019, she worked as an Engineer with the Hongdu Aircraft Design Institute of AVIC. Since 2020, she has been an Engineer with Yangzhou Academy of Collaboration & Innovation Company Ltd. Her research interests include top-level design, scheme design, POP, ICD, detail design of avionics system, UAV bee colonies, UAV obstacle avoidance technology, and manned and UAV coordinated operations.

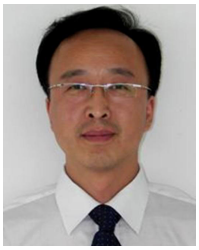

JIANBO LI received the M.Sc. degree and the Ph.D. degree in aerospace vehicle design from the Nanjing University of Aeronautics and Astronautics, Nanjing, China, in 2000 and 2003, respectively. From 2006 to 2008, he was an Assistant Professor with the National Key Laboratory of Rotorcraft Aeromechanics, Nanjing University of Aeronautics and Astronautics. He became a Full Professor, in 2009. His research interests include aerodynamics, flight dynamics and preliminary design of traditional helicopter, windmilling rotor aircraft, ducted fan aircraft, and rotor/wing compound aircraft.

YONGWEN YANG received the Bachelor of Engineering and the Master of Aircraft Design degrees from the Nanjing University of Aeronautics and Astronautics, in 2006 and 2011, respectively. He is currently working with Yangzhou Academy of Collaboration & Innovation Company Ltd. He is also a Senior Engineer. His main research interests include new concept aircraft market and demand analysis, overall scheme design.

YIBO LI received the Ph.D. degree in aircraft design from the Beijing University of Aeronautics and Astronautics, Beijing, China, in 2012. He is currently the Deputy General Manager and a Technical Director with Yangzhou Academy of Collaboration & Innovation Company Ltd. He is also a Researcher. His research interest includes overall design of the novel aircraft.